Journal of Vacuum Science and Technology A

RESEARCH ARTICLE | AUGUST 22 2024

Interpretation of complex x-ray photoelectron peak shapes. II. Case study of Fe $2p_{3/2}$ fitting applied to austenitic stainless steels 316 and 304

Special Collection: Reproducibility Challenges and Solutions II with a Focus on Surface and Interface Analysis

A. E. Hughes ; C. D. Easton ; T. R. Gengenbach ; M. C. Biesinger ; M. Laleh

J. Vac. Sci. Technol. A 42, 053206 (2024)
https://doi.org/10.1116/6.0003842

JVST A
Journal of Vacuum Science & Technology A
ARTICLE
pubs.aip.org/avs/jva

Interpretation of complex x-ray photoelectron peak shapes. II. Case study of Fe $2p_{3/2}$ fitting applied to austenitic stainless steels 316 and 304

Cite as: J. Vac. Sci. Technol. A **42**, 053206 (2024); doi: 10.1116/6.0003842
Submitted: 20 June 2024 · Accepted: 24 July 2024 ·
Published Online: 22 August 2024

View Online Export Citation CrossMark

A. E. Hughes,[1,2,a)] C. D. Easton,[3,b)] T. R. Gengenbach,[3] M. C. Biesinger,[4,5] and M. Laleh[6]

AFFILIATIONS

[1] Institute for Frontier Materials, Deakin University, Waurn Ponds, Geelong, 3216, Australia
[2] CSIRO, Minerals Resources, Private Bag 33, Clayton, VIC 3168, Australia
[3] CSIRO, Manufacturing, Private Bag 10, Clayton, VIC 3168, Australia
[4] Surface Science Western, The University of Western Ontario, London, Ontario N6G 0J3, Canada
[5] Department of Chemistry, The University of Western Ontario, London, Ontario N6A 5B7, Canada
[6] Australian Institute for Innovative Materials (AIIM), University of Wollongong, North Wollongong, NSW 2500, Australia

Note: This paper is part of the Special Topic Collection: Reproducibility Challenges and Solutions II with a Focus on Surface and Interface Analysis.

[a)] **Electronic mail:** Tony.Hughes@csiro.au
[b)] **Electronic mail:** chris.easton@csiro.au

ABSTRACT

In this paper, a review of the analysis of Fe $2p_{3/2}$ peak and other transition metals in the austenitic stainless steel literature is presented. It reveals the significant shortcomings of the most widely used approaches, based on the principle of "chemistry fitting," where single symmetric peaks are used to represent either individual oxidation states or specific compounds. No meaningful conclusions can be drawn from these commonly employed two- or three-component peak fitting (2C and 3C) approaches; the implication being that a large portion of the literature that relies on this approach is flawed. As a significantly more accurate and reliable alternative to "chemistry fitting," we also assess "envelope fitting" (using empirical multiplet structures) and examine its limitations when applying the approach to austenitic stainless steel data. A detailed comparison of these two fitting approaches is described in Part I. For other elements such as Cr 2p, the problems associated with using single components to represent oxidation states or compounds are not as severe. It was found that it does not impact binding energy measurements, but does influence relative intensities, which will have a flow-on effect for oxide thickness calculations and obtaining a correct understanding of the surface more broadly.

I. INTRODUCTION

X-ray photoelectron spectroscopy (XPS) is a widely used technique to investigate surface oxides such as passive layers on metals. As described in Part I,[1] XPS as a major surface characterization technique has been under development for several decades but despite the very substantial progress achieved in data processing and analysis the interpretation of XPS data of certain elements remains complex. Consequently, rather than just presenting spectra as collected, analysts often attempt to extract more information about the oxides contributing to the passive layer by fitting the spectra using single symmetric components. The most popular fitting approach is based on what can be described as "chemistry fitting," where each single symmetric component used in the fit, in the case of Fe $2p_{3/2}$, represents either an iron oxidation state or an iron compound, i.e., each component represents a contribution to the overall surface chemistry. However, this simple analysis approach was shown in Part I to provide no meaningful data. This has led, over time, to a situation where the literature is contaminated with poor data analysis which has become the norm in many fields.[2]

This is the case for passive film formation on iron and steels where surface composition, including in-depth profiles, has been determined using XPS based on the interpretation of transition metal core lines. The analysis of these core line spectra can be exceedingly difficult depending on the internal structure itself and the number of phases or oxidation states present in the sample. The core lines themselves are complex due to various physical processes that occur during photoemission including spin orbit splitting, multiplet splitting, Auger signals, and satellite peaks from shake-up, shake-off, plasmon loss peaks, as well as overlap with other peaks. In addition, there is still debate about how to treat the background beneath the peak of interest, arising, in part, from inelastically scattered electrons.

As demonstrated in Part I, a single oxidation state [e.g., Fe(II)] or a specific metal oxide (e.g., FeO) cannot be represented by a single symmetrical (or asymmetrical) standard Gaussian–Lorentzian [GL(x), where x is the fraction of the Lorentzian contribution] or Voigt profile, but is instead a complex peak shape that can extend over tens of eV in the region of interest for a peak. This often means that the experimentalist is dealing with the center of gravity of a complex peak, which may not always have a consistent position since it will vary with both internal structure of the compound including the influence of ligands and different levels of mixing of oxides/hydroxides in the layer itself.

In Part II, we draw on the analyses of model spectra used to undertake "envelope fitting" described in Part I to examine the XPS characterization of passive film formation on austenitic stainless steels 316 and 304 as a case study. The earliest example of envelope fitting derives from attempting to match the number of components under a peak to that determined using quantum mechanical calculations. For the Fe $2p_{3/2}$ peak, this is embodied in the experimental work of Grosvenor *et al.*[3] and Biesinger *et al.*,[4] which built on the calculations of Gupta and Sen.[5] Recently, this has evolved to accurately fitting the profile of pure compounds. The fit parameters obtained from each pure compound can then be applied to determine the relative fraction of each pure compound type present in a mixed composition material, e.g., determining the amount of Fe_3O_4, represented by a series of fit components with most parameters fixed, present in the mixed oxide on a austenitic stainless steel surface. While passive film formation on austenitic stainless steels may be considered a niche area, many of the lessons learnt by examining this area are transferrable to the broader context of how XPS is applied to other steels and to materials science in general. This paper focuses on a significant spread in reported binding energies (BEs) for Fe $2p_{3/2}$ in austenitic stainless steel, leading to equally widespread reporting of the metal oxidation states and/or iron species. In contrast, we demonstrate that there is far less ambiguity about the core level binding energies for Cr $2p_{3/2}$, Ni $2p_{3/2}$, and Mo $3d_{3/2}$.

This paper begins with a short section on austenitic steels and passive film formation. It then covers the methodology described in the literature for topics including surface preparation, BE referencing, and experimental details (Sec. III), respectively. The results for various core lines from austenitic stainless steels are dealt with in Sec. IV. This includes peak fitting details of Fe $2p_{3/2}$ and Cr $2p_{3/2}$ as well as some other metal lines in austenitic stainless steels reported in the literature. The spread of reported binding energies and species in the literature is then interpreted in terms of the envelope fitting approach, which employs multiplet components based on the work of Biesinger *et al.*[4] making a clear case that no meaningful data can be extracted from fitting oxides (e.g., FeO and Fe_2O_3) or oxidation states [e.g., Fe(II) and Fe(III)] using single symmetric peaks to represent either category. Other significant elements in stainless steel are then examined (Secs. IV C and IV D). In the case of chromium, the Cr 2p spectra are straightforward to interpret compared to Fe 2p and this is shown in the analysis below. Lastly, a general discussion of the results (Sec. V) and conclusions (Sec. VI) are presented.

II. AUSTENITIC STAINLESS STEEL

Passive film formation occurs on many metals and in some cases, such as austenitic stainless steels, provides enduring protection for the underlying metal. The formation and composition of passive films on stainless steels has been extensively studied using XPS. Based on these studies, the passive film is generally considered to have a duplex structure with an inner Cr-rich oxide layer, usually designated as Cr_2O_3, and an outer layer comprising mixed oxide and/or hydroxides based mainly on Fe oxides. This duplex structure was reported some time ago with Castle and Clayton recognizing that the outer layer (OL) has more dissolution products in the form of Fe compounds covering an inner Cr_2O_3 layer (IL).[6] Compositional changes in the passive layer when formed electrochemically were first reported in detail by Olefjord *et al.*[7] It should be noted that the term "passive layer" in austenitic stainless steel covers surface oxide formation under a range of conditions; some are formed simply by exposure to air/moisture, others electrochemically through anodic polarization, and others formed chemically or by heating. The different formation processes result in different phases being present on the surface, so proper Fe 2p analysis is essential to extract information about these phases.

The determination of the composition of the outer Fe-oxide layer relies predominantly on detailed analysis, using curve fitting, of the XPS Fe 2p region. Extracting oxidation state information from this region is one of the most difficult undertakings in XPS since it requires good treatment, both of the background underneath the peak, as well as explicit inclusion of multiplet and satellite structures in the fitting protocol.[3,4,8] For reasons detailed later, the Cr $2p_{3/2}$ and Ni $2p_{3/2}$ lines are less problematic. Suffice to mention here that these elements are generally present in one or two states only, i.e., Cr as Cr_2O_3 and Ni as metallic Ni, respectively.

The purpose of this study is to provide a critical review of the XPS analysis of passive layers formed on austenitic stainless steels as a case study in interpretation and reporting of complex XP spectra found in the literature. The choice of these materials is to limit the scope of the review because, first, the number of publications on surface oxides on ferrous metals is large and, second, as a group, these stainless steels have similar surface oxides.

III. METHODOLOGY

This section deals with how the data presented in the paper has been standardized for binding energy correction, which background corrections were used and the types of interferences that may occur in the spectra which need to be addressed. It also briefly examines other sources of variability in the data. The authors examined 93 papers for this review. The majority were identified using a Scopus search and the rest were identified from the literature contained in the papers identified using Scopus. The view of the authors is that this review covers most, if not all, of the scientific literature on austenitic stainless steels where fitting of the Fe $2p_{3/2}$ is presented. The analyses below assume that a monochromated x-ray source is used. Before the introduction of such sources, polychromatic sources were used, their use introducing secondary x-ray structures from the source. While these issues are not specifically addressed here, they can be accommodated in fitting using additional peaks.

A. Surface preparation

XPS probes the very top layers of a surface (up to 10 nm) and is therefore very sensitive to changes in the surface as well as surface contamination. Methods for the preparation of a clean surface were identified nearly 50 years ago by Castle and Clayton.[6] These methods detailed that (a) the existing surface oxide must be removed, (b) the method used to clean the surface must not cause selective elemental enrichment in alloys, and (c) re-oxidation prior to the development of the passive layer must be avoided. Based on such a protocol, a reproducible well-defined surface passive oxide can develop. This sequence should also include polishing down to submicrometer flatness to minimize any influence of surface roughness.

Unfortunately, this type of surface preparation is rarely being reported in the published literature, with careful preparation being largely confined to dedicated surface science studies. Instead, surface preparation is often subordinated to the basic preparation techniques used in electrochemistry, which usually relies on a rough polish (typically down to a 4000 grit, equivalent to 3 μm) on SiC or carborundum papers. This means that surface roughness will almost certainly contribute artifacts to measurements such as the thickness of oxide layers and surface composition. Additionally, XPS analysis is used postmortem and without supporting techniques to characterize precipitated products, which do not form a thin homogeneous layer on the surface. All these different degrees of preparation are reported in the literature.

B. Binding energy referencing

To compare binding energies between different studies, it is important to find a common reference between studies. Commonly, the C 1s of the main hydrocarbon peak observed for adventitious carbon (AdC)[9,10] is used and assigned a value of either 284.8 or 285.0 eV. Recently, Biesinger[9] reported an average value of 284.91 ± 0.25 eV for AdC, while other recent work by the authors on carbon steel preferred the use of the Fermi edge of Fe(0) for charge correction in which case the main peak of AdC was measured at 284.95 eV (unreported work). In this study, all C 1s values were corrected to 285.0 eV in cases where the C 1s binding energy is reported and other peaks adjusted accordingly. Charge referencing could be overcome by ensuring that authors collect and publish a scan of the Fermi edge for Fe(0); its position is more reliable than alternatives such as using adventitious carbon as the Fermi edge is directly related to the Fe(0) position.

C. Background subtraction

In general, the most commonly used background in the stainless steel literature is the Shirley background.[11–13] For many XP spectra, selecting the position for the boundaries of the background calculation is relatively straight forward being at a position, which represents the average of the noise on either side of the peak. In the case of first-row transition metals, the lower background limit is generally set just below the metal peak and the upper limit for most reports in the valley between the $2p_{3/2}$ and $2p_{1/2}$ peaks. The choice of the upper limit is arbitrary and is only chosen because this position is easily identified and it eliminates dealing with the complexities of the metal $2p_{1/2}$ and satellite structure above this position. In principle, of course, the background should be determined across the complete Fe 2p range and beyond.[14] In practice, this background is calculated only over the Fe $2p_{3/2}$ BE range of Fe 2p typically used for fitting, as shown in Fig. 1. Note that other features shown in Fig. 1, such as the Ni Auger spectrum, will be discussed below. Pauly *et al.*[15] demonstrated a method that calculates the background based on the inelastic-scattering cross section determined using the semiclassical dielectric response model for XPS and includes "all excitations caused by the moving photoelectron (including both bulk and surface excitations) as well as the shake-up processes caused by the suddenly created static core hole charge that gives rise to both plasmon excitations and excitations of electrons from occupied states to unoccupied states." This approach removes asymmetry associated with electron interactions with the material. The background determined by this method is close to the Shirley background.

D. Peak shapes

The literature on austenitic stainless steels overwhelmingly employs GL product functions as derived by Proctor and Sherwood.[13] Nowadays, a generalized Voigt-like function is commonly used as a peak model, particularly for cases where asymmetry is important,[16] such as for metal peaks, e.g., Fe(0). However, in the literature, the use of symmetric Lorentzian-heavy line shapes with undamped wings to obtain a good fit is a common occurrence. This is unrealistic, particularly on the lower BE side of the photoelectron peak. Some of the wing intensity may be accounting for the Ni Auger lines and Cr 2s instead of the Fe $2p_{3/2}$ peak.

In this paper, Gauss/Lorentz product lineshapes have been used in all fitting except the metal peak, following the original work by Biesinger *et al.* Metal peaks were fitted using a Voigt-like function [LA(1,2,10) from CASAXPS]. Typically, GL(70) (i.e., 70% Lorentzian) shapes were used for the multiplet components used for envelope fitting as reported previously, whereas GL(30) was applied where single component chemistry fits were used for compounds or oxidation states, i.e., reflecting the poor practice generally reported in the literature. The envelope fitting approach used the multiplets characteristics described by Biesinger *et al.* and is discussed in more detail in Part I. Briefly, photoionization generates unpaired electrons in the core levels and these electrons interact

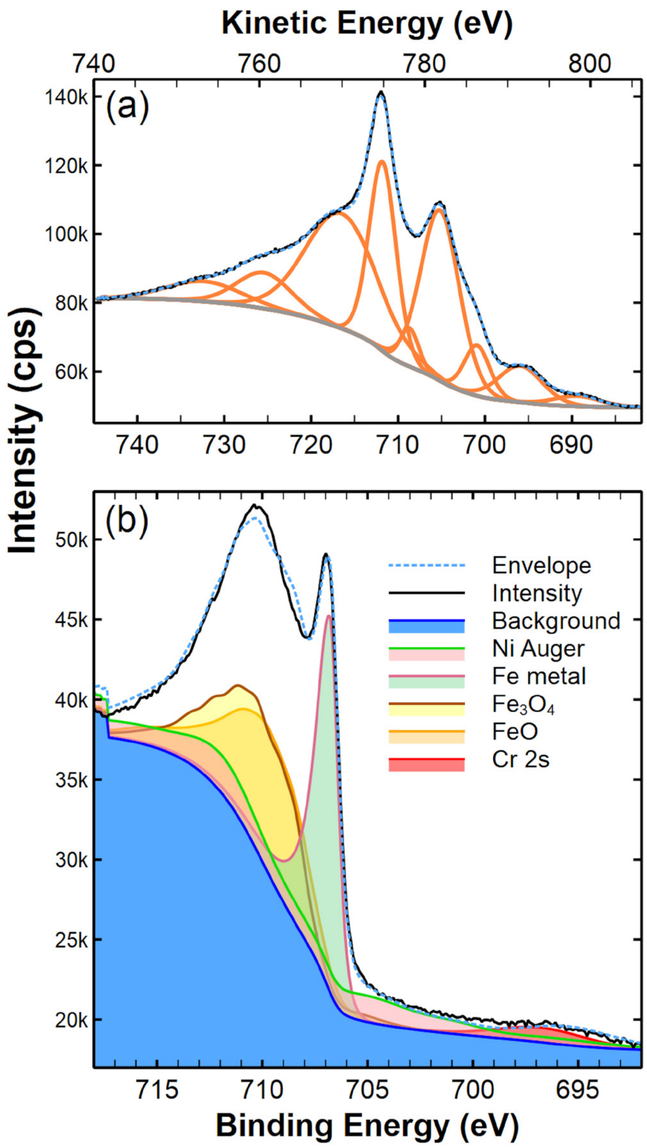

FIG. 1. (a) Ni $L_3M_{23}M_{23}$ Auger metal line fitted with 9 symmetric GL(30) product peaks that reproduce the Auger line profile collected from a Ni foil while simultaneously etching with an Ar^+ ion source. (b) The Fe $2p_{3/2}$ region from austenitic stainless steel including metal, oxides, Ni Auger, Cr 2s, and background. Only the sum of the multiplets for each oxide and the sum of the Auger peaks in (a) are presented. The peak positions have been calibrated against the Ni- and Fe-Fermi edges. An offset is used for the background at HBE, the magnitude determined by the intensity of the Ni Auger contribution around 704 eV.

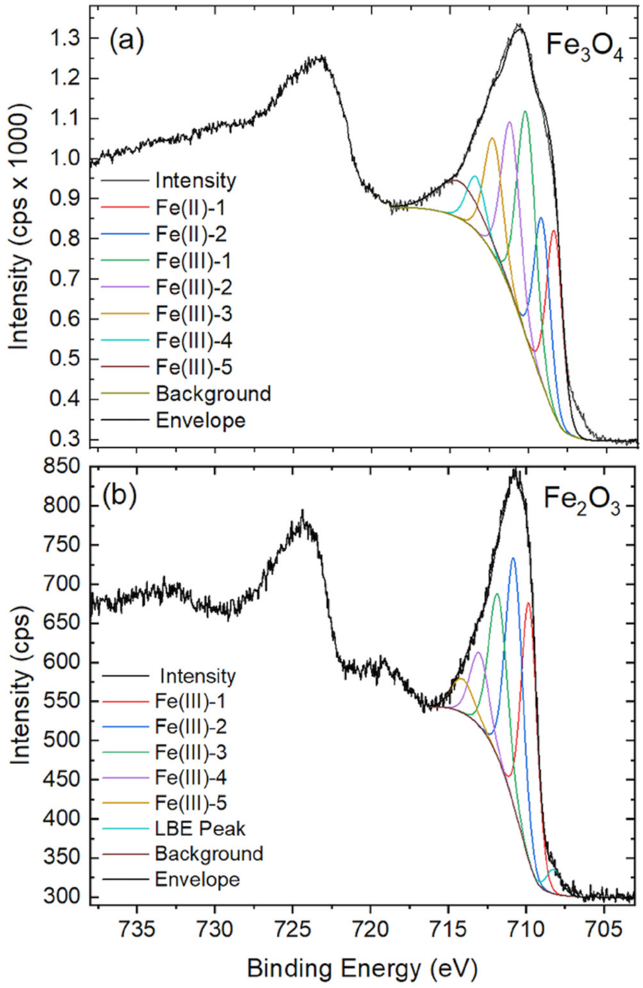

FIG. 2. Multiplet structure for (a) Fe_3O_4 and (b) Fe_2O_3 from Biesinger *et al.* (Ref. 4).

both with other unpaired electrons within the atom as well as electrons in ligand orbitals. The multiplet structure for FeO and Fe_2O_3 has recently been investigated by Bagus *et al.*[8,14] and for α-Fe_2O_3, γ-Fe_2O_3, $Fe_{3-\delta}O_4$, and Fe_3O_4 by Fujii *et al.*[17] It is important to recognize that there are literally thousands of multiplet peaks within the Fe 2p envelope. Bagus *et al.* rationalized the large number of multiplets to as little as 60 major multiplet states collected into 4 nearly degenerate (same energy) groups for FeO and 27 similarly collected into 4 groups for Fe_2O_3 over the binding energy range of the Fe $2p_{3/2}$ peak. They also demonstrated that there was significant intensity well outside this region, thus complicating both the spectroscopy of the Fe $2p_{3/2}$ peak (due to overlap with the $2p_{1/2}$ peak) and its quantification. There is also the additional uncertainty in determining the background underlying the peak as noted above.[8,18]

An example of this approach is shown in Fig. 2 displaying the semiempirical multiplet structure for envelope fitting developed by Biesinger *et al.*[4] for Fe $2p_{3/2}$ spectra of Fe_3O_4 and Fe_2O_3. The Fe $2p_{3/2}$ fit for Fe_3O_4 has seven peaks due to the presence of both Fe (II) and Fe(III) oxidation states in the compound expanding the overall range of the envelope, while the fit for Fe_2O_3 has five components. Note that the purpose of fitting to the reference compounds is to obtain a representative envelope of the Fe $2p_{3/2}$ peak which can be used to determine the percentage of that oxide in a sample with mixed oxides, it is not intended to extract an absolute intensity to determine an Fe/O ratio using both the Fe $2p_{3/2}$ and O 1s peaks. This means that satellite structures (e.g., feature at 718 eV in Fe_2O_3) are not necessary to include in the fitting as long as the background in all spectra is consistent. During fitting, only the area of all the components is scaled to a single component in the set, usually the most intense contribution, while all other component parameters including half width and relative position are fixed. This minimizes the number of components and parameters participating in the optimization process to a reasonable number. It can be seen that the envelopes derived from the multiplet fitting closely match the peak envelope.

E. Peak interference

Figure 1(b) presents a Fe $2p_{3/2}$ spectrum from stainless steel 316, together with labels of various elements and core lines demonstrating approximate positions relative to Fe 2p. The Auger lines identified, for Ni are applicable only when using an Al Kα anode, which is currently the most common x-ray source available on laboratory-based instruments. Overlapping from Auger lines can be especially problematic as they can have relatively intense, complex peak structures, as shown in Fig. 1(a) for Ni $L_3M_{23}M_{23}$. The influence of this Ni Auger on the Fe 2p of stainless steel contributes intensity across the whole Fe 2p region and can be identified at BEs lower than 700 eV superimposed on the normally flat background leading up to the Fe 2p peak.[19] If the aim is to fit the Fe $2p_{3/2}$ spectrum, then these contributions must be accounted for in the fit. This may require collecting reference data of such peaks from pure materials.

IV. RESULTS

In this section, the reported BE positions for fitting of the $2p_{3/2}$ photoelectron lines of the transition metals in the literature on austenitic stainless steel are reviewed and analyzed.

A. Fe $2p_{3/2}$ spectrum

The Fe $2p_{3/2}$ BE positions for various iron oxides/hydroxides reported in the literature are presented in Fig. 3. These BE values were referenced to a C 1s value of 285.0 eV where feasible, so it would be expected that all reported BE values for metallic Fe $2p_{3/2}$ be tightly grouped around the value 706.8 eV based on Biesinger *et al.*[4] (but adjusted from 284.8 to 285.0 eV). Generally, the metal BE values are consistent although there are outliers. The reasons for an observed deviation in the metal position may include

1. Poor spectrometer calibration,
2. Differential charging due to
   a. partial connection to the spectrometer, or
   b. inconsistent charge neutralization across the analysis region stemming from sample complexity such as corrosion products on the surface,

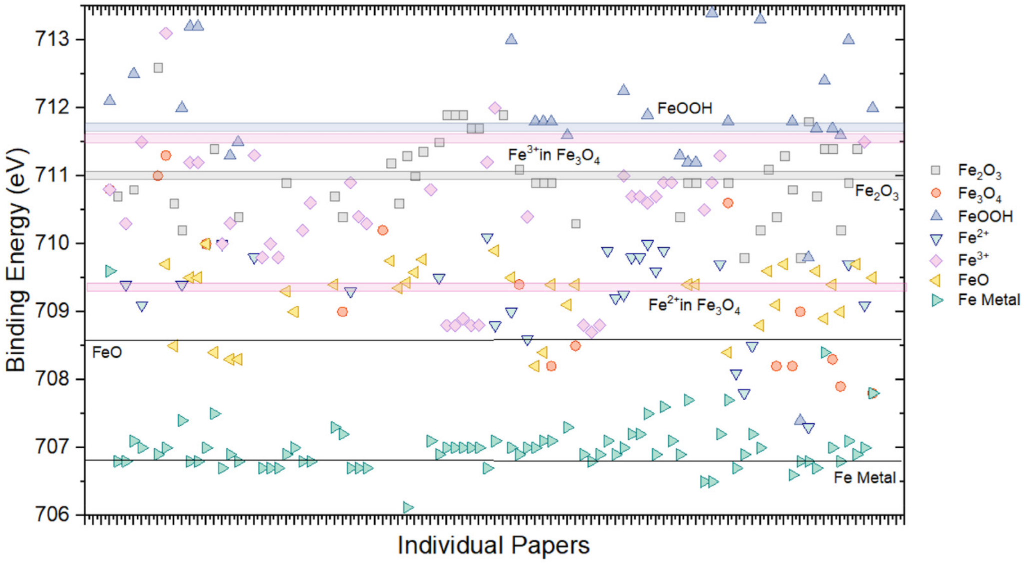

FIG. 3. Reported binding energy values for metallic iron and various iron oxide and hydroxides reported for the native and passive oxides formed on austenitic steels including SS316 and SS304. To provide a reference point for each assignment, values reported by Grosvenor *et al.* (Ref. 3) are included as a single line or colored bands (as labeled) based on their reported center of gravity of the multiplet structure. All positions have been adjusted to a C 1s value of 285.0 eV. NIST values: Fe (0) = 707.24 ± 0.88. FeOOH = 711.37 ± 0.27, Fe_2O_3 = 710.98 ± 0.39, Fe_3O_4 = 709.88 ± 1.11, FeO = 709.83 ± 0.47 (Ref. 21). Data obtained from the following citations: Refs. 7, 19, and 22–81. Note the same scales are used in Figs. 4, 6, and 8; thus, the values for Mo $3d_{5/2}$, Cr $2p_{3/2}$, and Fe $2p_{3/2}$ in austenitic stainless steels from each citation can be directly compared.

3. human error when performing charge correction,
4. or electronic effects (discussed below with respect to the Cr $2p_{3/2}$ peak).

Some of the variation seen in the values may be due to the absence of an internal C 1s reference and/or Au $4f_{7/2}$ was used instead. Commonly, gold (together with silver and copper) is used for calibrating the spectrometer, but it can only be used for charge correction if gold is evaporated onto the sample itself,[20] though this practice has its limitations.[10] Therefore, the assumption when using Au $4f_{7/2}$ is that the spectrometer is properly calibrated and there is a good electrical connection between the sample and the spectrometer ground.

Deviation from the Fe(0) value obviously means that there will be a corresponding uncertainty/error in establishing the BE position of oxidized Fe species, potentially leading to errors in the assignment of oxide species in the sample and hence the composition of the passive layer. Indeed, in Fig. 3, the magnitude of some of the variation of Fe(0) from the accepted value for the metal is similar in magnitude to the BE shift between different multiplet components and oxide positions.

With respect to the oxidized species in Fig. 3, the BE values reported by Grosvenor *et al.*[3] are highlighted by either a single line or thin colored bands (as labeled) based on the reported center of gravity of the multiplet structure.[82] It is clear there is little overall consistency or agreement in the literature about the assignment of species. Indeed, peak positions between 708.5 and 711.0 eV could be labeled as almost any oxide species, a scenario that can clearly lead to misidentification. As shown in Part I, this spread arises from using single peaks to fit multiplet structures in an attempt at a simplistic chemistry fit. In the case of Fe_3O_4, the Fe(II) multiplet structure for Fe^{2+} ions in Fe_3O_4 overlaps with the Fe(III) multiplet structure of Fe^{3+} ions in Fe_3O_4 leading to seven multiplet peaks in total spread over the BE range 709–715 eV based on the fitting protocol of Biesinger *et al.*[4] This means that the separation of Fe^{2+} and Fe^{3+} is impossible using only single components. This, of course, is further complicated when combinations of FeOOH, Fe_3O_4, Fe_2O_3, and FeO are present.

It is worth commenting here on the use of the NIST BE values recorded for various metals and oxide species. The NIST database compiles values from the literature for various metals and other species. Average binding energy values for positions of Fe $2p_{3/2}$, Cr $2p_{3/2}$, Ni $2p_{3/2}$, and Mo $3d_{5/2}$ species as taken from the NIST database are reported in Table I. In the case of Fe compounds, the average of these values has been corrected to the Fe $2p_{3/2}$ metal value of Biesinger *et al.*[4] (706.8 eV). Given that Fe $2p_{3/2}$ has many multiplets contributing to each oxide envelope, the question arises as to what NIST BE value should be assigned to Fe compounds. Prior to the publication of Grosvenor *et al.*[3] in 2004, the position of various Fe oxides and hydroxides would have been determined by the BE position of the peak maximum of each species. All the Fe_2O_3, Fe_3O_4, FeO, and FeOOH entries reported in the NIST database are pre-2004. This means that a center-of-mass value was likely reported for the BE rather than the positions of any of the individual multiplet components. Consequently, there is no simple way to connect the NIST value with the multiplet values reported by Biesinger *et al.*[4] Moreover, if there was some level of contamination of the samples in the early work, e.g., some hydroxide in the oxide, a common occurrence in XPS, then a further, undetermined error will be introduced to the BE position reported in the NIST database. Thus, in the case of high spin Fe compounds, the NIST values cannot be relied upon as a guide for identifying the nominated Fe species, yet these values are referred to in the literature.

B. Assessment of Fe $2p_{3/2}$ peak fitting for austenitic stainless steels

Based on the compilation of data presented in Fig. 3, it is obvious that there is a lack of consistency for the BE determination

TABLE I. Average NIST binding energies and standard deviations for multiple entries of various species, Biesinger and Grosvenor BE values are for the lowest multiplet and BE values for NIST entries corrected to Biesinger Fe(0) BE. (Note: values are corrected to C 1s = 285.0 eV).

Species	NIST (eV) (# of entries)	Std Dev. (eV)	Biesinger (eV) 1st multiplet	Grosvenor (eV) adjusted to 285.0 eV 1st multiplet and center of gravity (cog)	NIST corrected to Biesinger Fe(0) (eV)
Fe	707.24 (30)	0.88	706.8	—	0.44
FeO	709.83 (7)	0.47	708.4	708.3 (1st) 709.5(cog)	709.39
Fe_3O_4	709.88 (10)	1.11	708.4	708.4 (1st) 709.0 (cog)	709.44
Fe_2O_3	710.98 (20)	0.39	710.5	709.8 (1st) 710.9 (cog)	710.54
Fe(OH)O	711.37 (5)	0.27	710.9	710.2 (1st) 711.4 (cog)	710.93
Cr	574.17 (19)	0.25	574.2	—	—
Cr_2O_3	576.63 (41)	0.63	575.7	—	—
$Cr(OH)_3$	577.20 (26)	0.15	577.3	—	—
Ni	852.73 (35)	0.34	—	—	—
Mo	227.82 (24)	0.48	—	—	—
MoO_2	229.75 (15)	0.90	—	—	—
MoO_3	232.61 (22)	0.23	—	—	—

of Fe $2p_{3/2}$ across the austenitic stainless steel literature for values of oxide/hydroxide phases. This is due in part (i.e., in some papers[7,22,23,26–29,31,33,35,36,70,78,79,82–89]) to fitting of single symmetric peaks to extract each of Fe(II) and Fe(III) components and partly (in other papers[24,25,28,32,34,37,38,81,90,91]) due to using single symmetric peaks to fit individual compounds (e.g., Fe_2O_3 and Fe_3O_4); neither approach is appropriate. Consequently, nearly 100% of the values reported in the austenitic stainless steel literature are based on flawed analysis due to incorrect and/or poor approaches to fitting Fe $2p_{3/2}$ spectra and this practice is being propagated through the literature. In some instances, there is awareness of this issue with attempts to accommodate the multiplet structure by using a single asymmetric peak.[29,90]

As mentioned above, the source of the errors primarily lies in using single symmetric peaks for fitting complex peak envelopes. In the following, we look at how the details of this particular approach to fitting the Fe$2p_{3/2}$ peak leads to the spread in data presented in Fig. 3. To begin, the analysis of the Fe 2p peak in stainless steel involves before all else addressing the Ni-Auger lines. Generally, the amount of Ni in the passive layer is low due to the preferential oxidation of Cr and Fe in the alloy.[7,31] The general observation is that, as a result of the preferential oxidation, Ni enriches in the subsurface region in the metallic state, simplifying the analysis. However, this is not always the case and sometimes the electrolyte in which the passive layer is formed may cause Ni oxidation.[23] None of the papers surveyed state how they address intensity from the Ni Auger lines. A reasonable assumption would be that most authors are not aware of the contribution to the spectra. One consequence of this is that to accommodate the intensity resulting from the Ni Auger by using peak shapes with a considerable amount of Lorenztian character. The broad wings of the Lorentzian peak shape make allowance for additional intensity below the metal peak; this artificially increases the integrated intensity of the Fe$2p_{3/2}$ peak leading to an exaggerated spectral contribution from the Fe metal. It may also move the Fe $2p_{3/2}$ metal peak to lower binding energies.

Consequently, the first step to take in dealing with the Ni Auger contribution is to examine the Ni 2p spectrum to see if it is purely metal. Where metal is the only component (even the predominant component) then the Ni metal $L_3M_{23}M_{23}$ Auger line can be accounted for by using the components presented in Fig. 1 and listed in Table II. The objective in using these lines is simply to reproduce the Ni metal $L_3M_{23}M_{23}$ Auger envelope rather than to understand the underlying spectroscopy. When these components are used to fit Fe 2p spectra then it is necessary to fix the full width half maximum (FWHM) of each component, the intensities and position of each component relative to the first peak in the series, as described above and in Part I for envelope fitting. Overall, this means that only the intensity of the envelope is varied during an envelope fit. Ideally, the parameters in Table II should be determined experimentally to match the analysis conditions used. If oxidized Ni is also present, then an assessment of whether to include additional components related to the oxide must be made meaning appropriate control data of the Fe $2p_{3/2}$ region will be required. The Ni Auger line can be subtracted from the Fe $2p_{3/2}$ spectrum prior to any further processing as an alternative to including the Ni Auger envelope in the fit. Ni spectroscopy including Auger spectra for the pure oxide and hydroxide has been studied by Grosvenor *et al.*[92] and Biesinger *et al.*[93]

TABLE II. Ni $L_3M_{23}M_{23}$ Auger line components for reproducing the Auger line profile.

Position (eV)	Relative position (eV)	% Intensity	FWHM (eV)
689.4	0	1.79	6.414
695.93	6.53	5.85	5.96
700.90	11.51	4.69	3.45
705.16	15.76	23.97	5.22
708.69	19.29	2.63	2.54
711.78	22.38	18.57	3.65
716.51	27.14	29.91	9.68
725.41	36.01	7.14	7.42
732.33	42.93	5.45	10.072

Next is the analysis of the iron components to the Fe $2p_{3/2}$ peak itself. The shortcoming of the 2C and 3C methods, where no consideration is given to multiplet contributions, and simple symmetric (or asymmetric) peak profiles are used to extract chemical information were covered in Part I. In this section, we take the example of a Fe (0) + Fe_3O_4/FeOOH mix and see how BEs change with composition. The idea is to provide some insight into the large variability depicted in Fig. 3. Thus, Fig. 4 shows the BE positions for different components in the metal + 2C and metal + 3C fits to the series of data for metal + Fe_3O_4/FeOOH where the compositional mix of oxides is varied over the series. The BE position of the metal peak for both types of fits remains constant at around 706.5–706.7 eV across the whole composition range. For the metal + 2C fit, the low binding

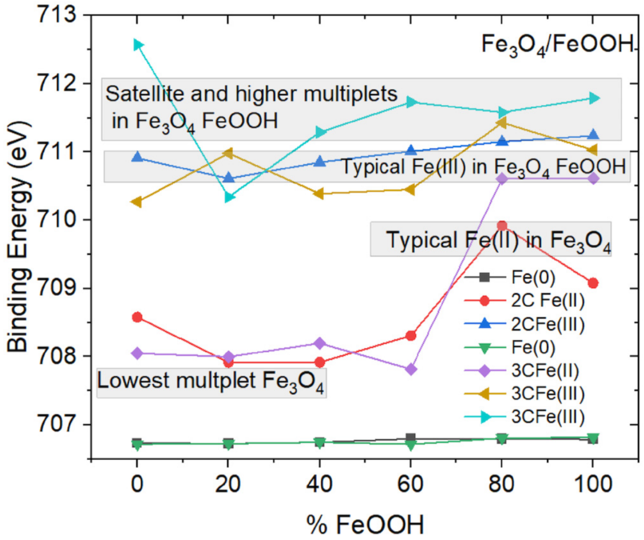

FIG. 4. Binding energy positions for GL(30) 2 component (2C) and 3 component (3C) fits to a series of spectra containing different mixes of Fe_3O_4 and FeOOH and metallic Fe.

energy (LBE) oxide component converges to values between 708 and 709 eV up to 60% FeOOH but then increases to approximately 709 to 710 eV at 80% FeOOH and above. Thus, even though there is still 40% Fe_3O_4 in the oxide composition, the LBE component no longer has any sensitivity to the Fe(II) signal from this region. The high binding energy (HBE) component converges to a value around 711 eV. The metal + 3C fits show a similar division between concentrations. The LBE component has similar values to the 2C fit up to 60% FeOOH then increases to around 710.6 eV close to 100% FeOOH. The two other components compete for intensity at binding energies between 710.5 and 712 eV.

It is interesting to look at these BE regions in terms of the multiplet and satellite structures of the two oxides involved. BE values around 708.5 eV reflect the lowest Fe (II) multiplet in Fe_3O_4 as seen in Fig. 2(a). It has no formal assignment as measured against the NIST database but is occasionally observed in the data reported in Fig. 3. In terms of envelope fitting, the contribution is unambiguously incorporated into Fe(II) multiplet components of the oxide and the envelope fitting approach accurately extracts the amount FeO or Fe_3O_4 as shown in Part I. Values for the HBE components could be assigned any of FeO, Fe_3O_4, FeOOH, or Fe_2O_3 from the NIST database. This ambiguity is reflected in the data in Fig. 3 where there is an enormous spread of assignments in this range. Values at 709.5 eV are typical of the 2nd Fe(II) multiplet in Fe_3O_4, and values above 710.5 eV reflect higher BE multiplets in Fe_3O_4 and FeOOH. Thus, the metal + 2C and 3C fits are converging to BEs that reflect the multiplet structures of these compounds, but do not accurately reflect these multiplet intensities and positions or indeed the oxide composition.

In practice, passive layers can frequently consist of more than two phases. For this reason, it is instructive to look at how well three oxide components can be fitted to the data using the envelope fitting approach. To assess this scenario, a model spectrum comprising 40% FeO, 40% Fe_3O_4, and 20% FeOOH was generated for the scenario of a relatively thick passive layer, i.e., no metal is seen in the XPS Fe $2p_{3/2}$ spectrum. An additional model containing 25% Fe metal (25% Fe metal, 30% FeO, 30% Fe_3O_4, and 15% FeOOH) was constructed for the case where some metal was observable through the oxide. The outcome of the fitting to these two models using the Biesinger envelope fit approach is depicted in Fig. 5.

In Figs. 5(a) and 5(b), only the fit envelopes are displayed for the three Biesinger components of FeO, Fe_3O_4, and FeOOH whereas the insets show the individual multiplet components obtained for the Monte Carlo error analysis. The breakdown of the percentages obtained for each component is presented in Table III using both the original Biesinger and modified Biesinger envelope components detailed in Part I. For the spectrum in Fig. 5(a), the fit using the envelope fit is able to recover the original composition within 2%. Moreover, the Monte Carlo error analysis [inset in Fig. 5(a)] shows that for multiple fitting with different starting points, the fitting converges to essentially the same results. This can give some confidence that when significant fractions of oxides/hydroxides are present in an Fe $2p_{3/2}$ spectrum, a good estimate of the composition can be obtained within the parameter space explored.

For the case where metal is also present in addition to three oxide components, the outcomes are not so encouraging. First, while the fit in Fig. 5(b) looks promising (low RMS and good reproduction of the spectral envelope), the actual breakdown of the percentage of each component does not accurately recover the original composition of the model spectrum. The metal and FeOOH percentages are overestimated, and the remaining two contributions are underestimated. In this case, the Monte Carlo error estimation shows that the fitting can converge to a wide range of solutions and, consequently, quantitative results would be unreliable. The outcome here is largely due to a loss of sensitivity for the lowest FeO multiplets in the BE range just above the metal peak. This means that during fitting there is not enough information to extract the FeO component accurately and intensity is lost from this peak but captured by the metal peak (Table III). This may also affect the fitting of the Fe_3O_4 component with some intensity from the Fe(II) multiplet structure being captured by the metal peak. This would lead to a lower estimate for the amount of Fe_3O_4 and a corresponding increase in the amount of FeOOH. In the case of the modified Biesinger components, the change in distribution of the intensities in these components better fits the metal and FeO regions, but the overestimation of the metal component leads to an underestimation of Fe_3O_4 and overestimation

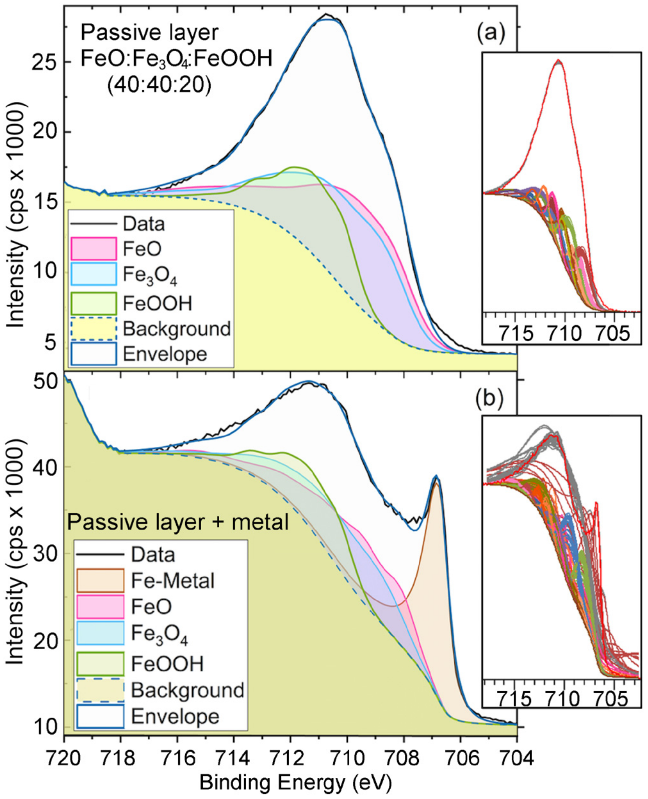

FIG. 5. Peak fitting of model passive layer Fe $2p_{3/2}$ spectra with three oxide contributions. Envelope fitting of spectrum containing (a) 40% FeO, 40% Fe_3O_4, and 20%FeOOH and (b) 25%Metal, 30% FeO, 30% Fe_3O_4, and 15%FeOOH. The insets represent Monte Carlo error analyses of the optimized fits. The color under the background is the sum of all colors under different peaks.

TABLE III. Percentage of Fe species obtained from fitting model oxide spectra and metal plus oxide spectra using envelope and chemistry fit approaches.

Envelope fit – % Intensity				
Components	Fe metal	FeO	Fe_3O_4	FeOOH
Model composition: $40FeO:40Fe_3O_4:20FeOOH$				
Biesinger	—	39.8	38.2	22.0
M-Biesinger	—	40.7	41.7	17.6
Model composition: $25Fe(0):30FeO:30Fe_3O_4:15FeOOH$				
Biesinger	30.1	18.3	25.2	26.4
M-Biesinger	22.8	29.7	20.8	26.7
2C and 3C chemistry fits – % Intensity and binding energies (eV)				
Components	Fe metal	1	2	3
Model composition: $40FeO:40Fe_3O_4:20FeOOH$				
2C %	—	53.3	46.7	—
BE	—	711.4	709.6	—
3C %	—	59.0	6.7	34.3
BE	—	711.7	708.4	710.1
Model composition: $25Fe(0):30FeO:30Fe_3O_4:15FeOOH$				
2C %	16.2	71.8	11.9	—
BE	707.5	710.5	706.7	—
3C %	13.4	73.0	1.2	12.5
BE	707.6	710.5	707.4	706.4

of FeOOH. These results suggest that the oxide composition cannot be determined when as much as 25% metal is present using available semiempirical approaches. The influence of the amount of Fe(0) is dealt with in more detail in Part I. One approach to dealing with this issue might be to collect data on the passive layer at low takeoff angles from the surface. In this case, data acquisition is more surface-sensitive with the effect of reducing the size of the metal component in the data.

The data for the 2C and 3C chemistry fits are also presented in Table III. In the case of the 2C fits to the oxide mix without metal, it is clear that the actual oxide mix cannot be recovered from the fitting. The mix of Fe(II) and Fe(III) is qualitatively close to the actual levels of Fe(II) and Fe(III), but the oxide composition could not be determined from this information. For the 3C fit, the low binding energy region has two peaks one of which converges to the lowest multiplet position of FeO and/or Fe_3O_4. Since the intensity of this peak is very low, it would not be possible to correctly determine the amount of either oxide. When the metal is present, the outcome from the 2C and 3C fits to the oxide components is worse. The second peak in the 2C fit and the second and third peaks in the 3C fit tend to converge to binding energies near the metal peak relegating the remaining intensity to the other oxide component in both cases. Clearly, the simplistic 2C and 3C chemistry fits generally lead to nonsense.

Applying these observations more generally to fitting of Fe $2p_{3/2}$ spectra obtained from the passive layer where no metal is present (thick passive oxide), the following observations can be made: When fitting two components to a spectrum, these two peaks (2C) will converge to positions straddling the positions of observed maximum intensity of the $Fe2p_{3/2}$ profile. Because a significant amount of intensity in the multiplet structure occurs at higher BE, the Fe(III) components of the 2C and 3C fits make the greatest contributions to this region and thereby dominate as a fraction of the total intensity. This can lead to the misidentification of the oxides present in the passive layer. The corollary of this analysis is that the spread of data seen in Fig. 3 for the literature is reflected in the 2C and 3C fitting presented in Fig. 4; since we have demonstrated that these simple fits do not represent the chemical makeup of the model spectra, it can be assumed that the data in Fig. 3 cannot be relied upon to reflect the composition of the coatings reported in individual studies. On the basis of the data presented here, the authors are advocating an approach based on envelope fitting as detailed in Part I, until fully developed theoretical approaches to Fe 2p fitting are available as readily deployable protocols to the practicing scientist.

A further observation made in Part I regarding problematic data processing reported in the literature concerns the strong satellite structure in Fe(III): there is an obvious intensity valley between the main Fe $2p_{3/2}$ peak and the satellite, which tends to be nominated as an endpoint for a Shirley background (this is, of course, quite arbitrary). This valley disappears with high levels of the Fe (II) component resulting in an apparent flat region between the $2p_{3/2}$ and $2p_{1/2}$ peaks and the endpoint for a Shirley background is more likely to be placed at higher BE. In analyzing a series of spectra, such a shift of background will lead to inconsistencies in data processing because moving the endpoint of the Shirley background will lead to the incorporation of additional intensity due to the larger processing region as noted in the literature.[94] This is particularly the case with satellite structure in FeOOH and Fe_2O_3 where there is clearly peak intensity in this region. In this case, reducing the height of the background at this point is required.

C. Cr $2p_{3/2}$ spectrum—where single component fitting almost works

Reported BE values for Cr $2p_{3/2}$ metal, Cr_2O_3 and $Cr(OH)_3$, are much more consistent when compared to those reported for Fe $2p_{3/2}$ across the range of papers reviewed in this study (Fig. 6). As for the Fe $2p_{3/2}$ analysis, the Cr $2p_{3/2}$ metallic peak should appear at the same position for all studies if the spectrometer is properly calibrated and the internal binding energy reference is the same across all studies. Indeed, this is generally the case (with some obvious outliers). The reason for these outliers has been covered above and may be due to spectrometer calibration, how charge correction was approached and internal reference standards which are not mentioned in all studies.

The data compiled in Fig. 6 indicate that the BE of Cr $2p_{3/2}$ for Cr(0) in the austenitic steels is, on average, slightly lower than that reported for the metallic state of the pure metal 574.4 eV (Ref. 4, corrected to C 1s at 285.0 eV). It is possible that this is an alloying effect compared to pure Cr. Batirev *et al.*[95] reported a charge transfer away from the atomic Fe sites during alloying. This charge transfer might produce greater screening of the core hole during photoionization at Cr sites in the alloy compared to pure Cr with the effect of lowering the binding energy.

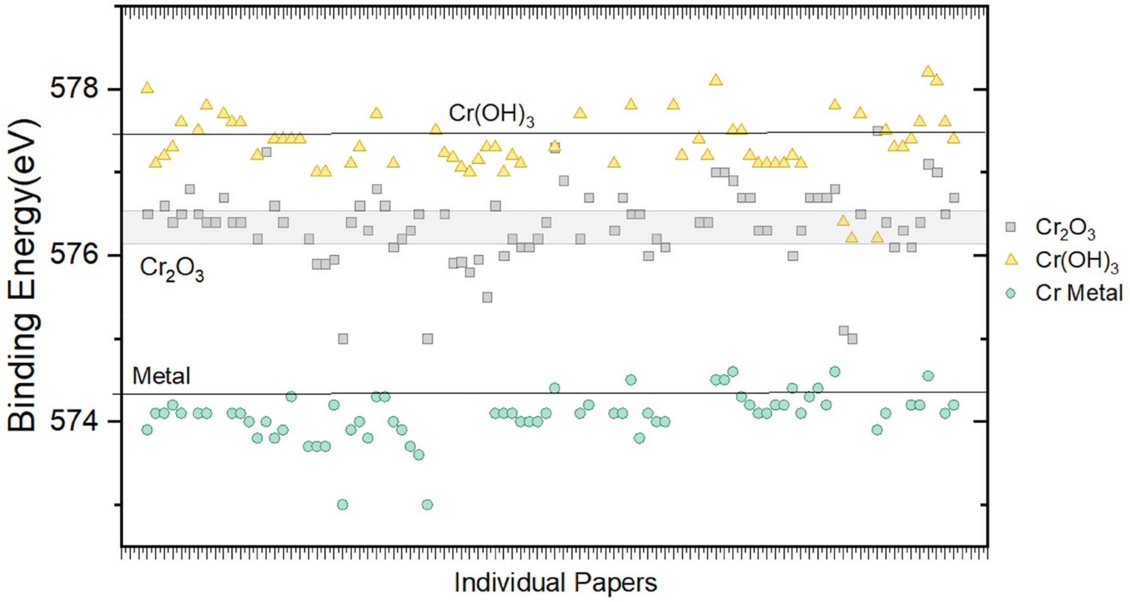

FIG. 6. Reported Cr 2p$_{3/2}$ binding energies for various species. Reference values represented by a single line Cr(0) or Cr(OH)$_3$ or gray band (Cr$_2$O$_3$) are based on the reported center of gravity of the multiplet structure taken from Biesinger *et al.* (Ref. 4): Cr metal has a single value and Cr$_2$O$_3$ has multiplet splitting so the range expresses where the center of gravity falls between the two largest multiplet peaks. The multiple structure for Cr(OH)$_3$ can be defined by a single symmetric peak. NB: The reference metal line is at 574.4 eV taken from Biesinger *et al.* (Ref. 4) but charge corrected using C 1s at 285.0 eV. NIST: Cr(0) = 574.17 ± 0.25 (n = 19), Cr$_2$O$_3$ = 576.63 ± 0.63 (n = 41), Cr(OH)$_3$ = 577.20 ± 0.15 (n = 8) (Ref. 21). Data obtained from following citations: Refs. 7, 19, 22, 23, 25–30, 32–38, 41–49, 52–58, 60–62, 65, 66, 68–76, 78, 80, 83, 84, 86, 89, and 96. Note the same scales are used in Figs. 3, 6, and 8; thus, the values for Mo 3d$_{5/2}$, Cr 2p$_{3/2}$, and Fe 2p$_{3/2}$ from each citation can be directly compared.

Cr$_2$O$_3$ and Cr(OH)$_3$ are the most commonly reported oxidized forms in passive layers. Biesinger *et al.*[4] reported five multiplet components for Cr$_2$O$_3$, while the multiplet structure for Cr(OH)$_3$ can be fitted with one broad (~2.5 eV FWHM) symmetric component. For Cr$_2$O$_3$, 70% of the intensity of the combined multiplets occurs in the first two multiplets. If these are used to indicate the peak position, then it should occur at 576.2 eV as depicted in Fig. 6. Indeed, the peaks reported in the literature are consistent with this value. Some insight into the question of why the peak position of the single component chemistry fit for Cr$_2$O$_3$ agrees so well with the Biesinger envelope fit can be seen in Fig. 7. Here, the multiplet components are filled in light gray and the envelope is shown as an orange outline. The single component (SC) chemistry fit is also depicted, in this case in a green outline. It is clear the peak position of the envelope falls at the same BE as the SC fit. Thus, this phase can be identified on the basis of the SC peak position. However, to accommodate the broadness and asymmetric distribution of the raw intensity, the optimization process tends to increase the FWHM of the SC Cr$_2$O$_3$ component to be greater than the FWHM of the envelope. This has a flow-on effect on the intensity of the Cr(0) component. While the component position is the same in both types of fits, the lower intensity means that it cannot be used for oxide thickness determination using a calculation based on exponential attenuation of the Cr(0) intensity as it will give an overestimate of the oxide thickness. Figure 7(b) shows the MC error analysis for both types of fits indicating that both are quite

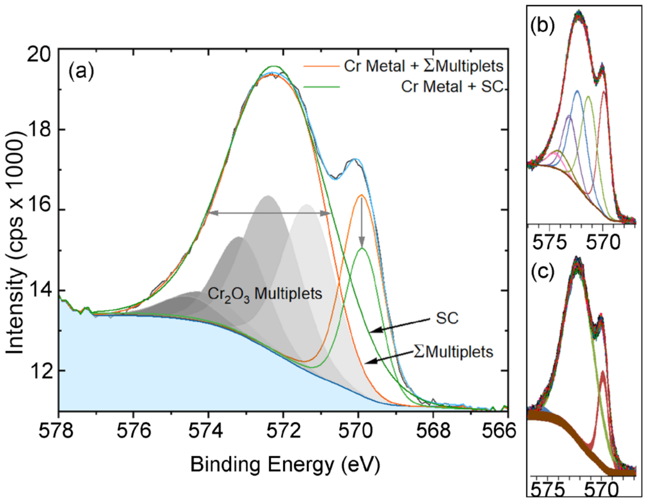

FIG. 7. (a) Cr 2p$_{3/2}$ spectrum featuring metal and Cr$_2$O$_3$ components using the fit parameters described in the work by Biesinger *et al.* (Ref. 4). Fitting shows two components in green [1x metal (smaller intensity component) + 1x oxide labeled SC] GL(30) chemistry fit and six components orange (1x metal (larger intensity component) + 1x Biesinger envelope labelled ∑Multiplets) fit. Note that the FWHM of the single oxide component is greater than the multiplet fit and that the metal component has a lower intensity. (b) and (c) represent Monte Carlo error analyses of the Biesinger envelope and 2C chemistry fits, respectively.

stable. The range of BE values for $Cr(OH)_3$ shows some spread between 577.2 and 577.5 eV, which is well within the reported range for this compound. Overall, the SC chemistry fit is deceptive, appearing to be a satisfactory fit as there is good agreement between the center of gravity of the two approaches. However, the GL(30) peak shape is not a good reproduction for Cr_2O_3 and thus an envelope fit is required to ensure correct intensities of the Cr phases are obtained.

D. Other elements

Of the remaining elements in austenitic steel, the most common transition elements are Ni, Mn, and Mo. With respect to nickel, it generally forms a subsurface enriched layer (due to preferential oxidation of Cr which forms the surface oxide and particularly preferential dissolution of Fe species in neutral to acidic media). Ni is therefore subsurface and in the metallic state. Oxidized Ni has been observed to be present in the outer oxide layer in basic solutions or under thermal oxidation of SS304L and to a lesser extent on SS316LN.[97] Because it is largely in the metallic state for which well-defined, fitting protocols are available, no detailed analysis is made here.

The only other commonly reported element is Mo in SS316L. Mo occurs in the passive layer in an oxidized state generally assigned to either Mo^{4+} or Mo^{6+}. The Mo $3d_{5/2}$ peak positions for these species are plotted in Fig. 8. Metallic Mo BEs published in the literature are generally consistent apart from a few outliers (Fig. 8). Values for MoO_2 and MoO_3 are also included along with the NIST standard values. The reported values for Mo^{4+} or Mo^{6+} appear to be similar or slightly lower (Fig. 8) compared to the average of the NIST values (and standard deviation for NIST values represented by the gray regions). Variation in the BE position might, in part, be due to referencing since many of the papers do not mention a C 1s reference value. Where it is mentioned, the values are very close to the averages for each species. However, if the correction was made using the Fe(0) values, which were 0.2 eV higher than the Biesinger Fe(0) values, then the Mo^{4+} or Mo^{6+} peaks would move to slightly lower values.

There is some discussion regarding fitting the Mo $3d_{5/2}$ of Mo^{6+} because MoO_3 degrades over time under the x-ray beam creating a Mo(V) species.[98] Approaches based on theoretical modeling have been used to guide the fitting procedure to experimental data.[98,99] It is also notable that Mo(IV) oxide shows screened and unscreened components that can complicate curve fitting.[99] In practice, most studies present data with poor signal to noise where more sophisticated approaches to data reduction would be undermined by the quality of the data. In summary, the absence of explicit C 1s reference value, low signal to noise, photoreduction of Mo(VI), and uncertainty in fitting procedures are probably all causes for some spread in the reported Mo $3d_{5/2}$ data.

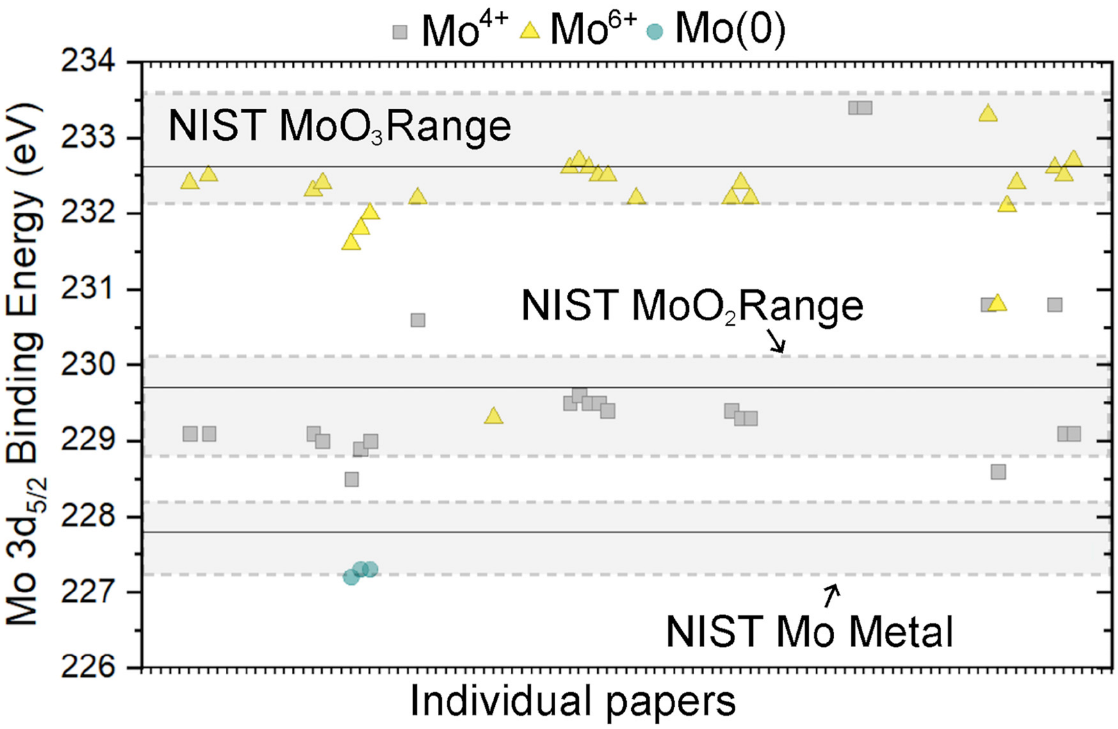

FIG. 8. Mo $3d_{5/2}$ reported peak positions for SS316 and single crystal studies where Mo is an alloying element. Lines indicate NIST values as reported in Table I and gray regions between dotted boundaries indicate the spread of NIST values. Many studies do not have a C 1s reference. Note the same x-scales are used in Figs. 3, 6, and 8; thus, values for Mo 3d5/2, Cr $2p_{3/2}$, and Fe $2p_{3/2}$ from each citation can be directly compared.

V. DISCUSSION AND RECOMMENDATIONS

The following discussion can be equally applied to the treatment of Fe $2p_{3/2}$ peak more generally as well as to the treatment of Fe $2p_{3/2}$ in austenitic stainless steel.

Based on our review of the literature, we conclude that the analysis of the Fe $2p_{3/2}$ peak is generally performed poorly. There is little attention paid to the physics of photoemission and the reason for using multiplet components and satellite structures. The variable quality of the treatment of XPS data in published papers means the reported compositions of the outer layer Fe oxides, based on these analyses, should be treated with skepticism. Moreover, since poor methodology is frequently being reported in papers that have been published in peer-reviewed, high-impact journals, those approaches are subsequently being used by other researchers and, thus, these erroneous procedures are being propagated in the literature. Fortunately, this is beginning to be understood more generally by individual researchers and scientific bodies and action is being taken.[100,101]

With respect to composition of the native iron oxides and passive layers reported in the literature, it can generally be concluded that compositions based on single component fits for speciation [e.g., Fe(II) and Fe(III)] or used to specifically define individual compounds should not be relied upon because peak assignment and particularly peak areas (used to calculate composition) are most likely in error. This conclusion also applies to depth profiles; thus, the depth distribution of Fe(II) and Fe(III) cannot be used to extract the chemical species because Fe(II) is present in both FeO and Fe_3O_4 at roughly the same binding energy and the Fe(III) component could comprise any or all of Fe^{3+} in Fe_2O_3, Fe_3O_4, and FeOOH. In addition, reduction of some oxides may occur through preferential etching of O groups under a high energy ion beam.[102] Moreover, this is also an issue for MoO_3 as discussed above.

Finally, a further complication of fitting the Fe $2p_{3/2}$ of austenitic stainless steels arises when using an Al Kα source because of interference of a complex Ni Auger spectrum with the Fe 2p spectrum as described above. In dual anode systems or synchrotron experiments, this peak can be moved by choosing a different anode or altering the incident x-ray energy. In the case of the Al Kα excitation source, the Ni Auger needs to be explicitly considered. Because the Ni content of stainless steels is around 10 wt. %, the Ni Auger will not give rise to peak structures with significant intensity, but without proper consideration might be included in the background thereby rendering the background incorrect and by extension any curve fitting. A previous study has shown that more than 80% of papers report using Al Kα,[103] indicating that it is likely the default x-ray source available to researchers in the study of Fe 2p of austenitic stainless steels and other materials.

While the work by Biesinger *et al.* is highly cited (+6000 citations at the time of writing), based on our observations the approach does not appear to be employed widely by the general materials science community. It is likely that many of these citations are relying on other information found in this publication such as BE positions for various metal oxides. As the work by Bagus *et al.* and others have shown, not only are we still far from a full theoretical treatment of iron oxide Fe 2p data, but it would also require the use and optimization of hundreds to thousands of multiplets if all are treated separately. In the absence of such a protocol, we have demonstrated the semiempirical treatment involving an envelope fit developed by Biesinger *et al.* with care and acknowledgment of the limitations of the method demonstrated in Part I and herein, can reproduce iron oxide compositions within 5% of their actual composition. In light of the abysmal performance of the popular chemistry fit based on 2C and 3C protocols, the Biesinger approach is a practical semiempirical method that can be utilized until a full theoretical treatment is available.

This review has clearly demonstrated that the analysis of Fe 2p spectra is poorly understood by many researchers, reviewers, and journal editorial staff. Having characterized the nature of the problem, it has enabled us to develop and offer strategies to deal with potentially problematic publications. The authors recommend following the schema presented in Fig. 9 in Part I with the accompanying detailed description. Using this schema, reviewers and editorial staff can assess the quality and reliability of XPS Fe $2p_{3/2}$ data. Following this schema also reinforces strict adherence to the principle that any published work should provide sufficiently comprehensive and detailed information to enable other researchers to reproduce the work. Many studies and the journals in which they are published fall well short of this principle.[103] This responsibility falls on authors as well as reviewers and particularly on journal editors. Thus, the top of the flow chart described in Part I (Fig. 9) deals with the basics, such as the method of binding energy calibration, spectrometer calibration, and interfering lines (e.g., Ni Auger). A comprehensive list of recommendations for the type of instrument and experimental parameters that should be reported when presenting XPS data in a paper have been detailed elsewhere.[103]

VI. CONCLUSIONS

In Part I, we demonstrated that commonly used approaches for fitting the Fe $2p_{3/2}$ peak as published in the literature are too simplistic. In our review, every paper that fitted XPS data employed these flawed methodologies based on two or three components. We have demonstrated that this is likely the main contributor to the significant spread of Fe $2p_{3/2}$ binding energy values reported for either Fe oxidation states or Fe compounds found in our review of the austenitic stainless steel literature.

Fitting of other components of austenitic stainless steels such as Cr $2p_{3/2}$ and Mo 3d is more easily handled. Using Biesinger *et al.*[4] envelope fitting for Cr_2O_3 will yield more accurate results for the intensity of both metal and Cr_2O_3 components compared to using only a single peak, though both approaches will yield similar results for BE positions. Because of the extensive use of these faulty methodologies to fit Fe $2p_{3/2}$ data in the literature, there appears to be a lack of awareness of the level of misinterpretation introduced by this approach to fitting. Accordingly, the authors report a protocol in Part I that can be used by authors, reviewers, and journal editors to assess the correctness of XPS in submitted papers. The protocol clearly describes what steps are available for fitting Fe $2p_{3/2}$ data. Part I also clearly outlines in which cases fitting of the Fe $2p_{3/2}$ peak does not yield reliable results; in those cases, the authors should avoid using peak fitting at all; publishing incorrect fitting results is worse than publishing no fitting results.

Overall, Parts I and II have demonstrated how poor XPS analysis has been allowed to propagate through the literature. The scientific method is fundamentally based on reporting of data and results that are based on proven, well-established, accurate, and reliable methods and protocols, supported by good statistics. In recent years, there has been a focus of journals to put much more importance on the techniques related to the field of the journal and less emphasis on ancillary techniques. This has created an environment where standards of scientific reporting for these ancillary techniques have degraded. In terms of passive layer composition, the impact has been incorrect reporting of oxide mixtures in passive layers with obvious flow-on effects. Clearly, this approach cannot be left to continue unabated; the authors must return to verifying the analysis methods they rely upon. Advances in analysis software have meant that many authors rely on the PABAGAR (press a button and get a result) approach rather than a deeper understanding of the technique they use. Reviewers and editors need to acknowledge that it is unlikely that they will be sufficiently proficient at all ancillary techniques and should seek assistance to fulfill their respective roles when evaluating every aspect of a paper.

ACKNOWLEDGMENTS

The authors thank Neal Fairley for assistance in the application of CASAXPS for the generation of the model spectra. The authors thank Don Baer for his valuable support and feedback.

AUTHOR DECLARATIONS

Conflict of Interest

The authors have no conflicts to disclose.

Author Contributions

A. E. Hughes: Conceptualization (equal); Data curation (equal); Formal analysis (equal); Investigation (lead); Methodology (equal); Writing – original draft (equal); Writing – review & editing (equal). **C. D. Easton:** Conceptualization (equal); Data curation (equal); Formal analysis (equal); Methodology (equal); Writing – original draft (equal); Writing – review & editing (equal). **T. R. Gengenbach:** Data curation (equal); Formal analysis (equal); Writing – original draft (equal); Writing – review & editing (equal). **M. C. Biesinger:** Writing – original draft (supporting); Writing – review & editing (supporting). **M. Laleh:** Conceptualization (equal); Data curation (supporting); Formal analysis (equal); Investigation (equal); Methodology (equal); Writing – original draft (equal); Writing – review & editing (equal).

DATA AVAILABILITY

The data that support the findings of this study are available within the article.

REFERENCES

[1] A. E. Hughes, C. D. Easton, T. R. Gengenbach, M. C. Biesinger, and M. Laleh, J. Vac. Sci. Technol. A **42**, 053205 (2024).
[2] G. H. Major *et al.*, J. Vac. Sci. Technol. A **38**, 6 (2020).
[3] A. P. Grosvenor, B. A. Kobe, M. C. Biesinger, and N. S. McIntyre, Surf. Interface Anal. **36**, 12 (2004).
[4] M. C. Biesinger, B. P. Payne, A. P. Grosvenor, L. W. M. Lau, A. R. Gerson, and R. S. Smart, Appl. Surf. Sci. **257**, 2717 (2011).
[5] R. P. Gupta and S. K. Sen, Phys. Rev. B **10**, 1 (1974).
[6] J. E. Castle and C. R. Clayton, Corros. Sci. **17**, 7 (1977).
[7] I. Olefjord, B. Brox, and U. Jelvestom, J. Electrochem. Soc. **132**, 2854 (1985).
[8] P. S. Bagus, C. J. Nelin, C. R. Brundle, B. V. Crist, N. Lahiri, and K. M. Rosso, J. Chem. Phys. **154**, 9 (2021).
[9] M. C. Biesinger, Appl. Surf. Sci. **597**, 153681 (2022).
[10] D. R. Baer *et al.*, J. Vac. Sci. Technol. A **38**, 3 (2020).
[11] J. Végh, J. Electron Spectrosc. Relat. Phenom. **151**, 3 (2006).
[12] J. Vegh, J. Electron Spectrosc. Relat. Phenom. **46**, 411 (1988).
[13] A. Proctor and P. M. A. Sherwood, Anal. Chem. **54**, 13 (1982).
[14] P. S. Bagus, C. J. Nelin, C. R. Brundle, B. V. Crist, N. Lahiri, and K. M. Rosso, Phys. Chem. Chem. Phys. **24**, 4562 (2022).
[15] N. Pauly, F. Yubero, J. P. Espinós, and S. Tougaard, Surf. Interface Anal. **51**, 353 (2019).
[16] G. H. Major, V. Fernandez, N. Fairley, and M. R. Linford, Surf. Interface Anal. **54**, 262 (2022).
[17] T. Fujii, F. M. F. de Groot, G. A. Sawatzky, F. C. Voogt, T. Hibma, and K. Okada, Phys. Rev. B **59**, 3195 (1999).
[18] M. Bravo Sanchez, J. A. Huerta-Ruelas, D. Cabrera-German, and A. Herrera-Gomez, Surf. Interface Anal. **49**, 253 (2017).
[19] M. Lampimäki, K. Lahtonen, P. Jussila, M. Hirsimäki, and M. Valden, J. Electron Spectrosc. Relat. Phenom. **154**, 69 (2007).
[20] A. E. Hughes and B. A. Sexton, J. Electron Spectrosc. Relat. Phenom. **50**, C15 (1990).
[21] A. V. Naumkin, A. Kraut-Vass, S. W. Gaarenstroom, and C. J. Powell, "X-ray photoelectron spectroscopy database," NIST, https://dx.doi.org/10.18434/T4T88K.
[22] D. Addari, B. Elsener, and A. Rossi, Electrochim. Acta **53**, 8078 (2008).
[23] M. Duportal, A. Oudriss, C. Savall, A. Renaud, C. Labrugère-Sarroste, and X. Feaugas, Electrochim. Acta **403**, 139684 (2022).
[24] W. Fredriksson, D. Petrini, K. Edström, F. Björefors, and L. Nyholm, Corros. Sci. **67**, 268 (2013).
[25] W. Fredriksson, S. Malmgren, T. Gustafsson, M. Gorgoi, and K. Edström, Appl. Surf. Sci. **258**, 5790 (2012).
[26] R. H. Jung, H. Tsuchiya, and S. Fujimoto, Corros. Sci. **58**, 62–68 (2012).
[27] R. H. Jung, H. Tsuchiya, and S. Fujimoto, ISIJ Int. **52**, 7 (2012).
[28] G. Lorang, M. D. C. Belo, A. M. P. Simões, and M. G. S. Ferreira, J. Electrochem. Soc. **141**, 3347 (1994).
[29] B. Lynch, S. Neupane, F. Wiame, A. Seyeux, V. Maurice, and P. Marcus, Appl. Surf. Sci. **554**, 149435 (2021).
[30] B. Lynch, Z. Wang, L. Ma, E.-M. Paschalidou, F. Wiame, V. Maurice, and P. Marcus, J. Electrochem. Soc. **167**, 141509 (2020).
[31] V. Maurice, H. Peng, L. H. Klein, A. Seyeux, S. Zanna, and P. Marcus, Faraday Discuss. **180**, 151 (2015).
[32] E. Menthe, K.-T. Rie, J. W. Schultze, and S. Simson, Surf. Coat. Technol. **74-75**, 412 (1995).
[33] S. Neupane, S. Zanna, A. Seyeux, L. H. Klein, V. Maurice, and P. Marcus, J. Electrochem. Soc. **169**, 011505 (2022).
[34] H. P. Qu, H. T. Chen, and Y. P. Lang, Constr. Build. Mater. **125**, 427–437 (2016).
[35] R. Robin, F. Miserque, and V. Spagnol, J. Nucl. Mater. **375**, 65 (2008).
[36] A. Rossi, B. Elsener, G. Hähner, M. Textor, and N. D. Spencer, Surf. Interface Anal. **29**, 460 (2000).
[37] D. Singh, D. A. Basha, A. Singh, R. S. Devan, and S. S. Hosmani, J. Mater. Eng. Perform. **29**, 10 (2020).
[38] L. Zeng, X. P. Guo, G. A. Zhang, and H. X. Chen, Corros. Sci. **144**, 258 (2018).
[39] C. Zhao, Y. Bai, Y. Zhang, X. Wang, J. M. Xue, and H. Wang, Mater. Des. **209**, 109999 (2021).
[40] Z. Duan, C. Man, C. Dong, Z. Cui, D. Kong, L. wang, and X. Wang, Corros. Sci. **167**, 108520 (2020).

[41] C. Man, C. Dong, J. Liang, K. Xiao, Q. Yu, and X. Li, Anal. Lett. **50**, 7 (2017).
[42] A. A. Hermas, Corros. Sci. **50**, 9 (2008).
[43] K. Bae, D. Shin, J. Lee, S. Kim, W. Lee, J. Ilguk, and J. Lee, Materials **15**, 18 (2022).
[44] L. Ma, F. Wiame, V. Maurice, and P. Marcus, Corros. Sci. **140**, 205–216 (2018).
[45] Z. Wang, E.-M. Paschalidou, A. Seyeux, S. Zanna, V. Maurice, and P. Marcus, Front. Mater. **6**, 232 (2019).
[46] W. Y. Lai, W. Z. Zhao, Z. F. Yin, and J. Zhang, Surf. Interface Anal. **44**, 5 (2012).
[47] L. Freire, M. J. Carmezim, M. G. S. Ferreira, and M. F. Montemor, Electrochim. Acta **55**, 6174 (2010).
[48] X. Yue, Z. Yang, L. Huang, L. Zhang, J. Li, Z. Xue, and J. Pan, J. Mater. Sci. Technol. **127**, 192–205 (2022).
[49] N. Le Bozec, C. Compère, M. L'Her, A. Laouenan, D. Costa, and P. Marcus, Corros. Sci. **43**, 765 (2001).
[50] W. P. Yang, D. Costa, and P. Marcus, J. Electrochem. Soc. **141**, 111 (1994).
[51] H. Luo, H. Su, C. Dong, and X. Li, Appl. Surf. Sci. **400**, 28–38 (2017).
[52] M. J. K. Lodhi, K. M. Deen, and W. Haider, Materialia **2**, 111–121 (2018).
[53] L. Wang, H. Tian, H. Gao, F. Xie, K. Zhao, and Z. Cui, Appl. Surf. Sci. **492**, 792–807 (2019).
[54] H. Luo, H. Su, G. Ying, C. Dong, and X. Li, Appl. Surf. Sci. **425**, 628–638 (2017).
[55] R. Jiang, Y. Wang, X. Wen, C. Chen, and J. Zhao, Appl. Surf. Sci. **412**, 214–222 (2017).
[56] S. Kumar, D. Jaiswal, C. K. Behera, and G. S. Mahobia, Mater. Chem. Phys. **290**, 126568 (2022).
[57] Y. Zhang, H. Luo, Q. Zhong, H. Yu, and J. Lv, Chin. J. Mech. Eng. **32**, 27 (2019).
[58] Y. Du, G. Yang, S. Chen, and Y. Ren, Corros. Sci. **206**, 110531 (2022).
[59] T. Cui, H. Qian, W. Chang, H. Zheng, D. Guo, C. T. Kwok, L. M. Tam, and D. Zhang, Corros. Sci. **218**, 111174 (2023).
[60] J. D. Choundraj, R. G. Kelly, R. Monikandan, P. M. Singh, and J. Kacher, Corros. Sci. **217**, 111098 (2023).
[61] R. Qi, X. Zhang, A. Wu, K. Sheng, and H. Lin, J. Clean. Prod. **389**, 136076 (2023).
[62] H. Xu, L. Wang, D. Sun, and H. Yu, Appl. Surf. Sci. **351**, 367–373 (2015).
[63] P. Qin, H. Ma, Y. Cui, R. Liu, P. Ju, F. Wang, and L. Liu, Corros. Sci. **223**, 111466 (2023).
[64] X.-Z. Wang, H. Luo, and J.-L. Luo, Electrochim. Acta **293**, 60–77 (2019).
[65] H. Krawiec, V. Vignal, O. Heintz, and R. Oltra, Electrochim. Acta **51**, 3235 (2006).
[66] M. Duportal, X. Feaugas, A. Oudriss, and C. Savall, Corros. Sci. **207**, 110546 (2022).
[67] J. Ma, B. Zhang, Y. Fu, X. Hu, X. Cao, Z. Pan, Y. Wei, H. Luo, and X. Li, Corros. Sci. **201**, 110257 (2022).
[68] G. Chen and C. R. Clayton, J. Electrochem. Soc. **144**, 9 (1997).
[69] E. De Vito and P. Marcus, Surf. Interface Anal. **19**, 403 (1992).
[70] K. M. Deen, M. J. K. Lodhi, E. Asselin, and W. Haider, J. Phys. Chem. C **124**, 39 (2020).
[71] Y. Gui, Z. J. Zheng, and Y. Gao, Thin Solid Films **599**, 64–72 (2016).
[72] M. Kumagai, S.-T. Myung, S. Kuwata, R. Asaishi, and H. Yashiro, Electrochim. Acta **53**, 12 (2008).
[73] K. Li, L. Liang, Q. Huang, J. Xiao, Y. Tian, and H. Wu, J. Mater. Sci. **57**, 1 (2022).
[74] K. Nakashima, A. Yamaguchi, Y. Kurono, Y. Sawae, T. Murakami, and J. Sugimura, Proc. Inst. Mech. Eng. J. **224**, 3 (2009).
[75] N. Padhy, R. Paul, U. Kamachi Mudali, and B. Raj, Appl. Surf. Sci. **257**, 5088 (2011).
[76] R. Pärna, E. Nõmmiste, A. Kikas, P. Jussila, M. Hirsimäki, M. Valden, and V. Kisand, J. Electron Spectrosc. Relat. Phenom. **182**, 108 (2010).
[77] Y. Sawae, K. Nakashima, S. Doi, T. Murakami, and J. Sugimura, in *Proceedings of the ASME/STLE International Joint Tribology Conference 2009, IJTC2009*, Memphis, TN, 19-21 October 2009 (American Society of Mechanical Engineers, New York, 2009), pp. 233–235.
[78] M. Shah, M. T. M. Ayob, N. Yaakob, Z. Embong, and N. K. Othman, Corros. Eng. Sci. Technol. **57**, 15 (2022).
[79] T. H. Wang, J. Wang, J. G. Bai, S. J. Wang, C. Chen, and P. D. Han, J. Iron Steel Res. Int. **29**, 6 (2022).
[80] Y. Yang, X. Ning, H. Tang, L. Guo, and H. Liu, Appl. Surf. Sci. **320**, 274–280 (2014).
[81] A. Kocijan, C. Donik, and M. Jenko, Corros. Sci. **49**, 2083 (2007).
[82] P. Marcus and M. E. Bussell, Appl. Surf. Sci. **59**, 7 (1992).
[83] Z. Wang, A. Seyeux, S. Zanna, V. Maurice, and P. Marcus, Electrochim. Acta **329**, 135159 (2020).
[84] Z. Wang, F. Di-Franco, A. Seyeux, S. Zanna, V. Maurice, and P. Marcus, J. Electrochem. Soc. **166**, 11 (2019).
[85] S. Jin and A. Atrens, Appl. Phys. A **46**, 1 (1988).
[86] Y. Yue, C. Liu, and M. Jiang, Steel Res. Int. **93**, 8 (2022).
[87] Y. Yue, C. Liu, P. Shi, and M. Jiang, Corros. Eng. Sci. Technol **53**, 3 (2018).
[88] C. Man, C. Dong, T. Liu, D. Kong, D. Wang, and X. Li, Appl. Surf. Sci. **467-468**, 193–205 (2019).
[89] L. Freire, M. A. Catarino, M. I. Godinho, M. J. Ferreira, M. G. S. Ferreira, A. M. P. Simões, and M. F. Montemor, Cem. Concr. Compos. **34**, 1075 (2012).
[90] M. Metikoš-Huković, Z. Grubač, and S. Omanovic, J. Serb. Chem. Soc. **78**, 12 (2013).
[91] Y. Yue, C. Liu, and M. Jiang, J. Mater. Eng. Perform. **32**, 9 (2023).
[92] A. P. Grosvenor, M. C. Biesinger, R. S. C. Smart, and N. S. McIntyre, Surf. Sci. **600**, 1771 (2006).
[93] M. C. Biesinger, L. W. M. Lau, A. R. Gerson, and R. S. C. Smart, Phys. Chem. Chem. Phys. **14**, 2434 (2012).
[94] C. R. Brundle and B. V. Crist, J. Vac. Sci. Technol. A **38**, 4 (2020).
[95] I. G. Batirev, J. A. Leiro, and M. H. Heinonen, J. Non-Cryst. Solids **197**, 205 (1996).
[96] T.-h. Wang, J. Wang, J.-g. Bai, S.-j. Wang, C. Chen, and P.-d. Han, J. Iron Steel Res. Int. **29**, 6 (2022).
[97] A. Stupnik, P. Frank, and M. Leisch, Ultramicroscopy **109**, 563 (2009).
[98] J. Baltrusaitis, B. Mendoza-Sanchez, V. Fernandez, R. Veenstra, N. Dukstiene, A. Roberts, and N. Fairley, Appl. Surf. Sci. **326**, 151 (2015).
[99] D. O. Scanlon, G. W. Watson, D. J. Payne, G. R. Atkinson, R. G. Egdell, and D. S. L. Law, J. Phys. Chem. C **114**, 4636 (2010).
[100] B. A. Sabel and R. Seifert, Naunyn-Schmiedeberg's Arch. Pharmacol. **394**, 2147 (2021).
[101] D. R. Baer, G. E. McGuire, K. Artyushkova, C. D. Easton, M. H. Engelhard, and A. G. Shard, J. Vac. Sci. Technol. A **39**, 2 (2021).
[102] B. A. Sexton, A. E. Hughes, and K. Foger, J. Catal. **77**, 85 (1982).
[103] G. H. Major, B. M. Clark, K. Cayabyab, N. Engel, C. D. Easton, J. Čechal, D. R. Baer, J. Terry, and M. R. Linford, J. Vac. Sci. Technol. A **41**, 4 (2023).